Measurement of $P_\mu\xi$ in Polarized Muon Decay version 3.5

B. Jamieson,[2] R. Bayes,[7,*] Yu.I. Davydov,[7,†] P. Depommier,[4] J. Doornbos,[7] W. Faszer,[7] M.C. Fujiwara,[7] C.A. Gagliardi,[6] A. Gaponenko,[1,‡] D.R. Gill,[7] P. Gumplinger,[7] M.D. Hasinoff,[2] R.S. Henderson,[7] J. Hu,[7] P. Kitching,[1] D.D. Koetke,[8] J.A. Macdonald,[7,§] R.P. MacDonald,[1] G.M. Marshall,[7] E.L. Mathie,[5] R.E. Mischke,[7] J.R. Musser,[6,¶] M. Nozar,[7] K. Olchanski,[7] A. Olin,[7,*] R. Openshaw,[7] T.A. Porcelli,[7,**] J.-M. Poutissou,[7] R. Poutissou,[7] M.A. Quraan,[1] N.L. Rodning,[1,§] V. Selivanov,[3] G. Sheffer,[7] B. Shin,[7,††] T.D.S. Stanislaus,[8] R. Tacik,[5] V.D. Torokhov,[3] R.E. Tribble,[6] and M.A. Vasiliev[6]

(TWIST Collaboration)

[1] *University of Alberta, Edmonton, AB, T6G 2J1, Canada*
[2] *University of British Columbia, Vancouver, BC, V6T 1Z1, Canada*
[3] *Kurchatov Institute, Moscow, 123182, Russia*
[4] *University of Montreal, Montreal, QC, H3C 3J7, Canada*
[5] *University of Regina, Regina, SK, S4S 0A2, Canada*
[6] *Texas A&M University, College Station, TX 77843, U.S.A.*
[7] *TRIUMF, Vancouver, BC, V6T 2A3, Canada*
[8] *Valparaiso University, Valparaiso, IN 46383, U.S.A.*

(Dated: May 8, 2006)

The quantity $P_\mu\xi$, where ξ is one of the muon decay parameters and P_μ is the degree of muon polarization in pion decay, has been measured. The value $P_\mu\xi = 1.0003 \pm 0.0006$ (stat.) ± 0.0038 (syst.) was obtained. This result is compatible with indirect measurements of $P_\mu\xi$, and confirms their implications for left-right symmetric models and other extensions of the Standard Model.

PACS numbers: 13.35.Bv, 14.60.Ef, 12.60.Cn

I. INTRODUCTION

In the Standard Model (SM) of particle physics, positive muons decay via the weak $(V-A)$ interaction into positrons plus neutrinos: $\mu \to e\nu\overline{\nu}$ through a virtual state involving W vector bosons. More generally, the amplitude for muon decay can be described in terms of a local decay matrix element, which is invariant under Lorentz transformations:

$$M = \frac{4G_F}{\sqrt{2}} \sum_{\substack{\gamma=S,V,T \\ \epsilon,\mu=R,L}} g^\gamma_{\epsilon\mu} \langle \bar{e}_\epsilon | \Gamma^\gamma | \nu \rangle \langle \overline{\nu} | \Gamma_\gamma | \mu_\mu \rangle, \qquad (1)$$

where the $g^\gamma_{\epsilon\mu}$ specify the scalar, vector, and tensor couplings between μ-handed muons and ϵ-handed positrons [1]. In the SM $g^V_{LL} = 1$, and all other coupling constants are zero.

The differential decay spectrum [2] of the e^+ emitted in the decay of a polarized μ^+ can be described by four parameters – ρ, δ, η and ξ – commonly referred to as the Michel parameters, which are bilinear combinations of the coupling constants. In the limit where the positron and neutrino masses are neglected, and radiative corrections [3] are not explicitly included, this spectrum is given by

$$\frac{d^2\Gamma}{dx d(\cos\theta)} \propto 3(x^2 - x^3) + \frac{2}{3}\rho(4x^3 - 3x^2) - P_\mu\xi\cos\theta(x^2 - x^3) - P_\mu\xi\delta\cos\theta\frac{2}{3}(4x^3 - 3x^2), \qquad (2)$$

where θ is the angle between the μ^+ momentum, which is opposite to the μ^+ polarization axis, and the outgoing positron direction, $x = E_e/E_{max}$ and P_μ is the degree of muon polarization. The fourth parameter, η, appears in the isotropic term when the positron mass is included in the analysis. In the SM, the Michel parameters take on the precise values $\rho = \delta = 0.75$, $\xi = 1$, and $\eta = 0$. For surface muons, produced from pion decays at rest, the SM magnitude of the polarization is $P_\mu = 1$. The parameter ξ expresses the level of parity violation in muon decay, while δ parametrizes its momentum dependence.

SM extensions involving right-handed interactions [4] require deviations from pure $V-A$ coupling that can alter $P_\mu\xi$. The non-negative quantity:

$$\begin{aligned} Q^\mu_R &= \frac{1}{4}|g^S_{LR}|^2 + \frac{1}{4}|g^S_{RR}|^2 + |g^V_{LR}|^2 + |g^V_{RR}|^2 + 3|g^T_{LR}|^2 \\ &= \frac{1}{2}[1 + \frac{1}{3}\xi - \frac{16}{9}\xi\delta], \end{aligned} \qquad (3)$$

sets a model independent limit on any muon right-handed couplings [1, 5]. A recent review of muon decay is presented in [6].

A precision measurement of muon decay can place limits on left-right symmetric (LRS) models [4]. In these

models both $V-A$ and $V+A$ couplings are present, and parity violation appears because of the difference in the mass of the vector bosons. The LRS models contain four charged gauge bosons $W_1^{\pm}$, $W_2^{\pm}$, the photon, and two additional massive neutral gauge bosons. The W_1 and W_2 masses are m_1 and m_2 respectively, and the fields W_L and W_R are related to the mass eigenstates W_1 and W_2 through a mixing angle ζ.

In the general LRS model [4],

$$\xi \sim 1 - 2\left[\left(\frac{g_R}{g_L}\frac{m_1}{m_2}\right)^4 + \left(\frac{g_R}{g_L}\zeta\right)^2\right], \qquad (4)$$

where g_R and g_L are the right- and left-handed gauge couplings. The manifest left-right symmetric model makes the additional assumptions that $g_R = g_L$ and that the left- and right-handed quark mixing matrices are identical. In this case, P_μ can also be expressed in terms of m_1/m_2 and ζ, and one obtains [4]:

$$P_\mu\xi \approx 1 - 4\left(\frac{m_1}{m_2}\right)^4 - 4\zeta^2 - 4\left(\frac{m_1}{m_2}\right)^2\zeta. \qquad (5)$$

Recently the TWIST collaboration reported new measurements of ρ [7] and δ [8]. In this paper a new measurement of $P_\mu\xi$ is reported. Prior to TWIST, the most precise direct measurement of $P_\mu\xi$ was 1.0027 ± 0.0079 (stat.) ± 0.0028(syst.) [9], in agreement with the SM. A similar value has been measured using muons from kaon decay [10]. Using the result $P_\mu\xi\delta/\rho > 0.99682$, at the 90% confidence level [11], along with the TWIST measurements of ρ and δ, an indirect limit on $P_\mu\xi$ was determined to be $0.9960 < P_\mu\xi \leq \xi < 1.0040$ (90% confidence level) [8].

II. EXPERIMENTAL PROCEDURES

In the present experiment, highly polarized surface muons [12] were delivered, in vacuum, to the TWIST spectrometer [13] by the M13 channel at TRIUMF [14]. The surface muon beam was produced with a typical rate of 2.5 kHz, and a momentum bite, $\Delta p/p \approx 1.0\%$ FWHM.

The TWIST spectrometer [13] was designed to measure a broad range of the normal muon decay spectrum, allowing the simultaneous extraction of the spectrum shape parameters. The spectrometer consists of 56 very thin high precision chamber planes, perpendicular to the axis of a solenoid producing a magnetic field of 2 T. For this measurement a 71 ± 1 μm thick, 99.999% pure, Al target was used. The decay positrons spiral through the chambers producing hits on the wires, which are recorded by time-to-digital converters. These helical tracks are subsequently reconstructed and analyzed to determine the positron energy and angular distributions. The momentum resolution is typically 100 keV/c, and the $\cos\theta$ resolution is about 0.005 [7]. The reconstruction and event selection techniques are identical to [8].

A low pressure (8 kPa dimethyl ether gas) removable beam monitoring chamber [15] provided information on the muon beam before it traversed the fringe field of the solenoid. The chamber consisted of two modules, one to measure the position and divergence of the muon beam in the horizontal (x) direction, and the other for measurements in the vertical (y) direction.

The solenoid field was found to interact with the iron of the beamline magnets, such that the muon beam was deflected off axis. Changing the angle of the beam relative to the magnetic field axis gives rise to a change in the polarization along the z axis of the stopped muons. The available M13 channel magnets could only partially alleviate the deflection of the beam, in the x direction.

Control of the muon stopping position in z ($\bar{z}_\mu$) was provided by feedback of $\bar{z}_\mu$, from online analysis, to the fractions of He and CO_2 in a gas degrader. The analysis quantity $\bar{z}_\mu$, used in the feedback loop, was the average z from the last chamber plane fired by the muons.

III. DATA ANALYSIS

TWIST determines the Michel parameters by fitting two-dimensional distributions of reconstructed experimental decay positron momenta and angles with distributions of reconstructed simulated data [8]. In bringing the muon beam to a stop at the center of the TWIST spectrometer, the muons are depolarized by the combination of multiple scattering, interaction with the fringe field of the spectrometer, and interactions when stopped in the high purity Al target. Thus, the polarization of the muon with respect to the z axis when it decays, P_μ^d, is lower than its polarization with respect to the muon momentum when it was produced in pion decay. To obtain an absolute measurement of $P_\mu\xi$, data are fit to a simulation that includes effects of fringe field depolarization and material depolarization.

Determining the positron momentum and angle is done with a chi-squared fit to a helical track that includes the drift time information from each cell. The efficiency of the track fitting is $\gtrsim$99.5% within the nominal fiducial region used for spectrum fitting [7, 8].

The energy calibration of the decay positrons is obtained from a fit to the endpoint of the spectrum. The endpoint fit function is a slope with an edge convoluted with a Gaussian. The corrected momentum $p_{\rm ec}$ is given by:

$$p_{\rm ec} = p_{\rm rec}\left(1 + \frac{\beta}{p_{\rm edge}}\right)^{-1} + \frac{\alpha}{|\cos\theta|}, \qquad (6)$$

where $p_{\rm rec}$ is the reconstructed momentum, $\cos\theta$ is the reconstructed cosine of the decay positron angle, $p_{\rm edge}$

is the maximum positron momentum, β defines the momentum scale related to the magnitude of the spectrometer magnetic field, and $\alpha = (\alpha_u, \alpha_d)$ is the zero angle energy loss for upstream (u) or downstream (d) decay positron tracks. This simple form is valid to first order because of the planar geometry of the wire chambers. The end point of the muon decay spectrum and sections of the 2-dimensional end point fit function for the bins within the fiducial region with the smallest upstream and downstream angles are shown in Fig. 1. The difference in yield between upstream and downstream emphasizes the asymmetry of polarized muon decay.

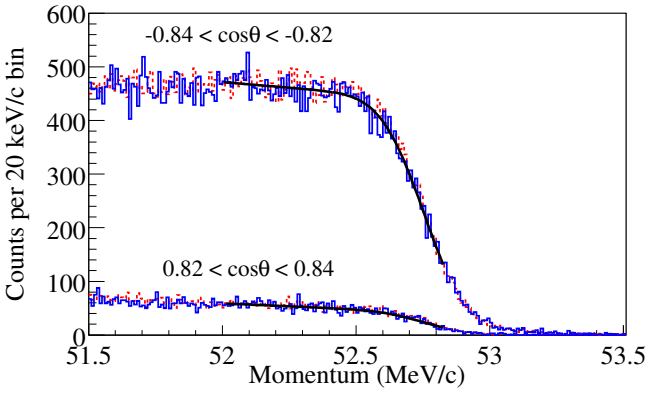

FIG. 1: (colour online) Sections of the 2-dimensional end point fit function of the muon decay spectrum for the bins within the fiducial region containing the smallest upstream and downstream angles. The data are shown as a solid-line, the matching simulation set is shown as a dashed-line, and the endpoint fit functions are shown as smooth curves.

The endpoint fit parameter β is highly correlated with $\alpha_{\rm sum} = \alpha_u + \alpha_d$. In the simulation the momentum is measured without bias at the few keV/c level, the magnetic field is measured with an NMR probe, and the magnetic field map has been determined to better than 0.2 mT in the tracking region. For this reason the endpoint fits are done with the value of β set to zero and assigned an uncertainty consistent with the momentum fit and field map accuracy. A 12 keV/c difference between the data and simulation $\alpha_{\rm sum}$ values was observed, and this is corrected by applying the energy calibration.

The TWIST simulation is based on GEANT 3.21 [16] and the chamber response is based on a space to time relation calculated with GARFIELD [17]. The simulation contains virtually all the components of the spectrometer with which a muon or a decay positron could interact. The output exactly mimics the binary files generated by the data acquisition system. Details of the simulation have been presented previously [7, 8].

The main factors that influence the muon polarization are the transport of the muon spins in the various regions of magnetic field and models for the muon depolarization in materials. Transport of the muon spins is done using a classical fourth order Runge-Kutta using the Nystroem algorithm [18], of the Bargmann-Michel-Telegdi [19] equation. The inherent accuracy of this numerical integration is negligible when compared to the accuracy of its result which depends more critically on the knowledge of the input beam parameters and the magnetic field map. For this reason, the beam monitoring chamber measurements were used to generate the muon beam for the simulation. The magnetic field map of the solenoid, used in simulation and analysis, was derived from a finite element analysis model, which includes the fringe field region.

A blind analysis is implemented by utilizing hidden Michel parameters ρ_H, δ_H, and ξ_H to generate the simulated decay rate. The decay rate can be written as:

$$\left.\frac{d^2\Gamma}{dx d(\cos\theta)}\right|_{\rho_H,\delta_H,\xi_H} + \sum_{\lambda=\rho,\xi,\xi\delta} \frac{\partial}{\partial\lambda}\left[\frac{d^2\Gamma}{dx d(\cos\theta)}\right]\Delta\lambda,$$

because the decay spectrum is linear in the shape parameters. The simulation spectrum is fit to the data spectrum by adjusting the $\Delta\lambda$.

The fiducial region adopted for this analysis requires $p < 50$ MeV/c, $|p_z| > 13.7$ MeV/c, $p_T < 38.5$ MeV/c, and $0.50 < |\cos\theta| < 0.84$. The fiducial cuts, while intentionally chosen to be conservative, are related to physical limitations of the TWIST detector. The 50 MeV/c momentum cut rejects events that are near the region utilized in the energy calibration. It is also important to avoid the region very close to the end point to minimize the sensitivity of the Michel parameter fits to details of the simulation that may affect the momentum resolution. The longitudinal momentum constraint eliminates events with helix pitch near the 12.4 cm periodicity in the wire chamber spacing. The transverse momentum constraint ensures that all decays are well confined within the wire chamber volume. The angular constraint removes events at large $|\cos\theta|$ that have worse resolution and events at small $|\cos\theta|$ that experience large energy loss and multiple scattering. These limits were fixed early in the analysis. The value of $P_\mu\xi$ was found to change by less than 0.0001 when the fiducial boundaries were moved by $\pm 2\%$ in momentum cut values and $\pm 10\%$ in $|\cos\theta|$ cut values.

An alternate analysis scheme, used only to compare relative polarizations, was developed using an integral asymmetry defined as the difference between the number of forward and the number of backward decays divided by their sum. To obtain a polarization estimate the forward and backward sums were done inside the fiducial region described in the previous paragraph and normalized using integrals of Equation 2 with the SM values of the Michel parameters inserted.

IV. EVALUATION OF SYSTEMATICS

The leading systematic uncertainties in this measurement of $P_\mu\xi$ arise from the potential sources of muon depolarization. These include depolarization due to the production target and beamline, fringe field depolarization, and interactions with material while the muon is propagating through the detector and after stopping.

The depolarization in the production target is due to multiple scattering of the muons while exiting the target. The muons in the beam arise from a maximum depth of 0.003 cm of graphite, which contributes only 0.2×10^{-3} to the systematic uncertainty in $P_\mu\xi$.

The muon polarization with respect to the beam and solenoid axis is reduced as the beam traverses the fringe field of the solenoid due to the increase in transverse momentum. The uncertainty in the muon polarization due to this phenomenon is dominated by uncertainties in the knowledge of the beam properties. This is estimated from the different settings used in data taking for the second dipole element (B2) in the M13 channel. The beam parameters were measured for two different B2 settings, both before and after the data collection. The beam measurements from after the data-collection match each of the four beam settings (B2+0.5 %, nominal, aperture, and high rate) used in this measurement of $P_\mu\xi$. The relative changes in angle and position between the nominal B2 value (94.4 mT) and B2+0.5 % settings are similar, but the absolute numbers for the average beam angles are quite different. This could be due to changes in the performance of the beam monitoring chamber or to its alignment to the beamline. To determine the sensitivity of the polarization to beam position and angle, a simulated beam was scanned in position and angle and the polarization was found to depend quadratically on the input variables. Using this parameterization, the predicted polarizations for the four characterization runs are shown in Table I. The larger of the differences in predicted polarization for a given B2 setting (0.0033) is adopted as an estimate of the uncertainty due to lack of reproducibility of the beam parameters.

TABLE I: Average beam positions and angles from beam monitoring measurements taken at different times, along with the simulation estimates of the muon polarization. The first (last) two entries are from before (after) the data collection.

B2 (mT)	$\bar{x}$ (cm)	$\bar{\theta_x}$ (mrad)	$\bar{y}$ (cm)	$\bar{\theta_y}$ (mrad)	$P_\mu^{\rm sim}$
94.4	0.07	-5.9	0.97	7.0	0.9929
94.9	0.85	-1.1	0.87	-5.0	0.9955
94.4	0.06	-6.7	0.73	-11.2	0.9941
94.9	0.94	-1.5	0.64	-19.2	0.9922

Uncertainties due to deconvolution of the beam angle measurement, modeling of the shape of the solenoid fringe field, and beam size reproduction also contribute to the final quoted systematic uncertainty of 0.0034 due to fringe field depolarization.

The depolarization of the muons while they propagate through the detector and interact with the detector materials is believed to be negligible [20]. Most muons stop in the high-purity Al target, where they can interact with conduction electrons. These electrons create a large hyperfine magnetic field at the site of the muon, which can be considered as a fluctuating local field with a correlation time $\tau_c \simeq 10^{-13}$ s in Al [21]. This short correlation time results in a Korringa depolarization rate [22] that has an exponential form, and does not depend on the magnetic field. Significant depolarization rates of $\lambda > 0.001\ \mu{\rm s}^{-1}$ have been measured for muons in Cd, Sn, Pb, As, Sb, and Bi [23]. The authors explained the measured depolarization rates to be due to Korringa depolarization because the λ values increase with temperature as predicted.

Jodidio *et al.* [11] measured a depolarization rate of $(0.43\pm0.34)\times10^{-3}\ \mu{\rm s}^{-1}$ for their Al target at 1.1 T. This rate is about 2.5σ smaller than the $(1.55 \pm 0.28) \times 10^{-3}$ $\mu{\rm s}^{-1}$ observed in this experiment. The difference could partly be due to the 2.5 to 5.5% of the muons that stop in the gas before our stopping target. The functional form of the depolarization in gases is more complex, but it can be approximated by an exponential or Gaussian form [22].

The difference between Gaussian and exponential extrapolations of the integral asymmetry measurement, as shown in Fig. 2, is 2.4×10^{-3}. Half the difference is the *correction* applied to the simulation to data fits, because the simulation was generated with a Gaussian form, while in reality the shape is most likely a linear combination of a Gaussian and exponential. An estimate of the extrapolation uncertainty is half the difference between the Gaussian and exponential extrapolations.

Other systematic uncertainties were studied by employing the fitting technique described in the data analysis section. In this case the fits are of experimental data (or simulation) samples, taken with a systematic parameter set at an exaggerated level, to data (or simulation) taken under ideal conditions. The difference measured, or sensitivity, expresses the changes in the spectrum shape caused by the systematic effect in terms of the changes in the Michel parameters. Systematic uncertainties in the measurement of $P_\mu\xi$ are summarized in Table II.

Several of the systematic uncertainties could vary from data set to data set and are denoted by (ave), and are considered data set dependent when calculating the weighted average value of $P_\mu\xi$. For example, the effect of positron interactions on upstream and downstream decay positrons changes when the mean muon stopping location is adjusted; thus the systematic uncertainty in $P_\mu\xi$ due to positron interactions is set-dependent.

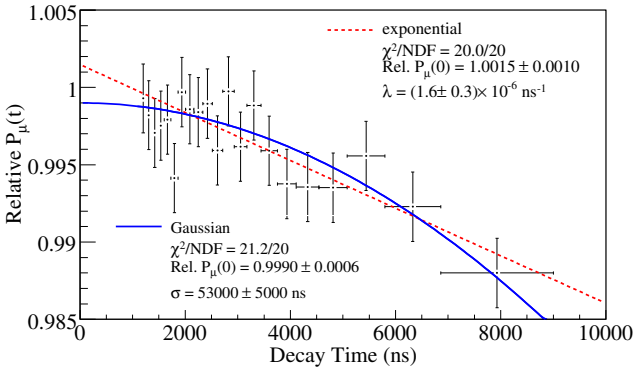

FIG. 2: (colour online)Extrapolation to zero decay time of relative muon polarization, estimated using the decay positron integral asymmetry described in the text. The extrapolation function is fit to data: with an exponential shown as a dashed-line, and as a Gaussian shown as a solid-line. Data before 1 μs are not considered because of possible contamination of late TDC hits from muons for upstream decay positrons.

TABLE II: Contributions to the systematic uncertainty for $P_\mu\xi$.

Effect	Uncertainty
Depolarization in fringe field (ave)	0.0034
Depolarization in stopping material (ave)	0.0012
Chamber response (ave)	0.0010
Spectrometer alignment	0.0003
Positron interactions(ave)	0.0003
Depolarization in production target	0.0002
Momentum calibration	0.0002
Upstream-downstream efficiency	0.0002
Background muon contamination (ave)	0.0002
Beam intensity (ave)	0.0002
Michel parameter η	0.0001
Theoretical radiative corrections	0.0001

V. RESULTS

The result for $P_\mu\xi$ presented here uses a data sample consisting of 2×10^9 events recorded in Fall 2004. This data sample includes eight data sets, of which seven were used for the extraction of $P_\mu\xi$. Each of the seven data sets used different beam characterization profiles that matched different conditions under which the data were recorded. The remaining data set was used to determine the detector response using decay positrons from muons stopping in the trigger scintillator and the first few chamber planes (far upstream), as described in [7, 8].

Five sets of data were taken with the beam steered nominally. One data set had the muon beam stopping with the Bragg peak centered in the target (stop $\frac{1}{2}$). Two sets, which were separated in time by a few days, were taken with the muon Bragg peak shifted to 3/4 of the way through the Al stopping target (stop $\frac{3}{4}$ A, B). One set was taken with a muon beam size limiting aperture (aperture), and one set was taken with the beam rate increased (high rate).

TABLE III: Results for $P_\mu\xi$. Each fit has 1887 degrees of freedom. Statistical and set-dependent systematic uncertainties are shown. A description of the data sets is in the text.

Data Set	$P_\mu\xi$ ± stat ± syst	χ^2
B2+0.5%	1.0023 ± 0.0015 ± 0.0037	2007
PC5 stop	1.0055 ± 0.0030 ± 0.0038	1906
stop $\frac{1}{2}$	1.0015 ± 0.0014 ± 0.0037	1876
stop $\frac{3}{4}$ A	0.9961 ± 0.0014 ± 0.0037	1900
high rate	0.9997 ± 0.0019 ± 0.0037	1932
aperture	0.9978 ± 0.0018 ± 0.0037	1896
stop $\frac{3}{4}$ B	1.0009 ± 0.0019 ± 0.0037	1841

Two sets of data were collected with the beam displaced by changing the last bending magnet (B2) field by +0.5% from nominal. One of the data sets (B2+0.5%) had the muon Bragg peak centered in the stopping target, while in the other set (PC5 stop), the muons were stopped relatively far upstream in order to increase the relative fraction of muons stopping in gas. All of these data sets, using different beam characterization profiles that matched the different conditions, were used in this determination of $P_\mu\xi$.

The spectrum fit results for the parameter $P_\mu\xi$ are presented in Table III. At the present stage TWIST cannot provide an improved measurement of η, therefore its value is set to the global analysis value of -0.0036 [24], to constrain the other parameters better. The uncertainty of ± 0.0069 on the accepted value of η gives an uncertainty of ± 0.0001 on the final value of $P_\mu\xi$.

The average values of ρ and δ from the present fits are 0.749 and 0.753, respectively. An evaluation of the uncertainties in ρ and δ has not been performed, but if one assumes systematic uncertainties similar to the previous TWIST measurements, these values are consistent with the published values of ρ [7] and δ [8].

To illustrate the quality of the fit, and how the spectrum fit distinguishes between $P_\mu\xi$ and $P_\mu\xi\delta$, the contribution to the fit asymmetry versus momentum for each of these terms and from the best fit $A(p)$ are shown in Fig. 3. Note that the total asymmetry versus momentum, $A(p)$, is the sum of the asymmetries due to each of the terms that have a $\cos\theta$ dependence:

$$A(p) = A_\xi(p) + A_{\xi\delta}(p). \quad (7)$$

The top panel in Fig. 3 shows the best fit asymmetry versus positron momentum, $A(p)$ with all of the fiducial cuts applied as a solid line; the contribution to the fit from the ξ term as a long-dashed line; and the contribu-

tion to the fit from the $\xi\delta$ term as the short-dashed line. The bottom panel shows the difference, $\Delta A(p)$ between data and fit.

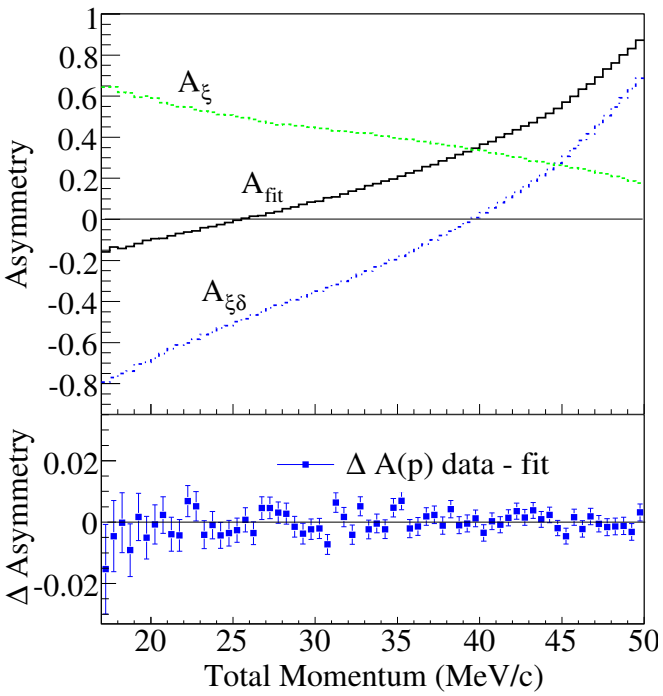

FIG. 3: (colour online) The top panel shows the fit asymmetry versus positron momentum, $A(p)$, along with the contributions to the fit $A(p)$ from ξ and $\xi\delta$ terms. The bottom panel shows the difference between the data and fit, $\Delta A(p)$.

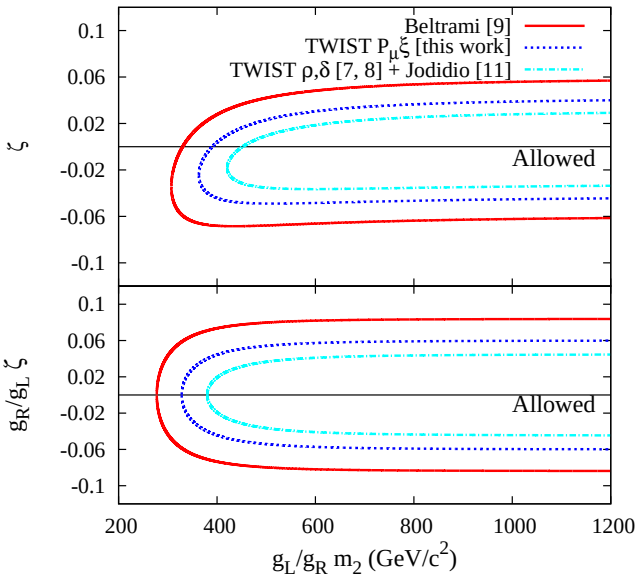

FIG. 4: (colour online) The top panel shows the manifest LRS model 90 % confidence limits on ζ and m_2 ($g_L/g_R = 1$) from measurements of $P_\mu\xi$. The bottom panel shows the same limits in the general LRS model case.

VI. CONCLUSION

The value of $P_\mu\xi$ was found to be 1.0003 $\pm$ 0.0006(stat.) $\pm$ 0.0038(syst.). The central value for $P_\mu\xi$ was calculated as a weighted average using a quadratic sum of the statistical and set-dependent uncertainties for the weights. The final systematic uncertainty is a quadratic sum of the set-independent and the average values of the set-dependent systematics.

The measured value of $P_\mu\xi$ is slightly greater than one. Thus there are no most likely values of the LRS model parameters; only limits can be determined. Also, because the measured value of $P_\mu\xi$ is consistent with one, there is no evidence for, or against, LRS models. The new limits on the LRS model parameters, ζ and m_2, are shown in Fig. 4.

The central value measured is closer to the SM value than previous direct measurements, and, hence, in a global fit with all other muon decay parameter data [24] it pulls those parameters that are sensitive to $P_\mu\xi$ (Q_{RR}, Q_{LR}) closer to the SM value. The changes are small compared to the uncertainty on these parameters. The present result reduces the uncertainty on the direct measurement of $P_\mu\xi$ [9] by a factor of two; it is also consistent with the SM and the value obtained indirectly [8]. This is TWIST's first measurement of $P_\mu\xi$, and prospects for reducing the main systematic uncertainties in $P_\mu\xi$ for data taken in the future are excellent.

We would like to thank C.A. Ballard, M.J. Barnes, J. Bueno, S. Chan, B. Evans, M. Goyette, A. Hillairet, K.W. Hoyle, D. Maas, J. Schaapman, J. Soukup, C. Stevens, G. Stinson, H.-C. Walter, and the many undergraduate students who contributed to the construction and operation of TWIST. We thank D.G. Fleming and J.H. Brewer for discussions on muon spin interactions in condensed matter. We also acknowledge many contributions by other professional and technical staff members from TRIUMF and collaborating institutions. This work was supported in part by the Natural Sciences and Engineering Research Council and the National Research Council of Canada, the Russian Ministry of Science, and the U.S. Department of Energy. Computing resources for the analysis were provided by WestGrid.

* Affiliated with: Univ. of Victoria, Victoria, BC.
† Affiliated with: Kurchatov Institute, Moscow, Russia.
‡ Present address: LBNL, Berkeley, CA.
§ Deceased.
¶ Present address: Arkansas Tech University, Russellville, AR.

** Present address: Univ. of Manitoba, Winnipeg, MB.
†† Affiliated with: Univ. of Saskatchewan, Saskatoon, SK.

[1] W. Fetscher, H.-J. Gerber and K.F. Johnson, Phys. Lett. B **173**, 102 (1986).
[2] L. Michel, Proc. Phys. Soc. A **63**, 514 (1950); C. Bouchiat and L. Michel, Phys. Rev. **106**, 170 (1957); T. Kinoshita and A. Sirlin, Phys. Rev. **108**, 844 (1957).
[3] A.B. Arbuzov, Phys. Lett. B **524**, 99 (2002); JHEP **03**, 063 (2003); JETP Lett. **78**, 179 (2003); A. Arbuzov, A. Czarnecki and A. Gaponenko, Phys. Rev. D **65**, 113006 (2002); A. Arbuzov, and K. Melnikov, Phys. Rev. D **66**, 093003 (2002).
[4] P. Herczeg, Phys. Rev. D **34**, 3449 (1986).
[5] S. Eidelman *et al.*, Phys. Lett. B **592**, 1 (2004).
[6] Y. Kuno and Y. Okada, Rev. Mod. Phys. **73**, 151 (2001).
[7] J.R. Musser *et al.* (TWIST Collaboration), Phys. Rev. Lett. **94**, 101805 (2005).
[8] A. Gaponenko *et al.* (TWIST Collaboration), Phys. Rev. D **71**, 071101(R) (2005).
[9] I. Beltrami *et al.*, Phys. Lett. B **194**, 326 (1987).
[10] J. Imazato *et al.*, Phys. Rev. Lett. **69**, 877 (1992).
[11] A. Jodidio *et al.*, Phys. Rev. D **34**, 1967 (1986); **37**, 237(E) (1988).
[12] A.E. Pifer, T. Bowen, and K.R. Kendall, Nucl. Instr. and Meth. **135**, 39 (1976).
[13] R.S. Henderson *et al.*, Nucl. Instr. and Meth. A **548**, 306 (2005).
[14] C.J. Oram *et al.*, Nucl. Instr. and Meth. **179**, 95 (1981).
[15] J. Hu *et al.*, submitted to Nucl. Instr. and Meth., (2006).
[16] R. Brun *et al.*, GEANT3 Users Guide, CERN Program Library W5013 (1994).
[17] R. Veenhof, GARFIELD, Version 7.10.
[18] E. J. Nystrom, Acta Soc. Sci. Fenn., 50, No.13, 1-55 (1925).
[19] V. Bargmann, L. Michel, and V. L. Telegdi, Phys. Rev. Lett. **2**, 435 (1959).
[20] M. Senba, J. Phys. B: At. Mol. Opt. Phys. **31**, 5233 (1998).
[21] A. Abragam, The Principles of Nuclear Magnetism, Oxford, 335 (1961).
[22] J. Korringa, Physica **16**, 601 (1950).
[23] S.F.J. Cox *et al.*, Physica B **289-290**, 594 (2000).
[24] C.A. Gagliardi, R.E. Tribble, and N.J. Williams, Phys Rev. D **72**, 073002 (2005).